CHAPTER 2

SIMPLIFIED ANALYTICAL PROCEDURES FOR PREDICTING SOIL-STRUCTURE INTERACTION EFFECTS

2.1 Introduction and Problem Definition

2.1.1 Components of the Soil-Structure Interaction Problem

The deformations of a structure during earthquake shaking are affected by interactions between three linked systems: the structure, the foundation, and the geologic media underlying and surrounding the foundation. A seismic Soil-Structure Interaction (SSI) analysis evaluates the collective response of these systems to a specified free-field ground motion.

Two physical phenomena comprise the mechanisms of interaction between the structure, foundation, and soil:

- *Inertial Interaction*: Inertia developed in the structure due to its own vibrations gives rise to base shear and moment, which in turn cause displacements of the foundation relative to the free-field.
- *Kinematic Interaction*: The presence of stiff foundation elements on or in soil will cause foundation motions to deviate from free-field motions. Three mechanisms can potentially contribute to such deviations: (a) Base-Slab Averaging; free-field motions associated with inclined and/or incoherent wave fields are "averaged" within the footprint area of the base-slab due to the kinematic constraint of essentially rigid-body motion of the slab, (b) Embedment effects; the reduction of seismic ground motion

with depth for embedded foundations, and (c) Wave Scattering; scattering of seismic waves off of corners and asperities of the foundation.

The effects of these phenomena are often described by a complex-valued transfer function relating free-field and foundation motions, and a complex-valued impedance function which quantifies the stiffness and damping characteristics of foundation-soil interaction. The damping represented by the imaginary part of the impedance function is a consequence of hysteretic damping in the soil and foundation, and radiation of seismic energy away from the foundation through the soil.

Both the transfer and impedance functions are dependent on the finite stiffness and damping characteristics of the soil medium. For the fictional condition of an infinitely stiff soil, the amplitude of the transfer function for translational motion is unity and the phase is zero (i.e. the foundation and free-field motions are identical), and the impedance function has infinite real parts and zero imaginary parts. It is of some practical significance that this unrealistic assumption of rigid soil is made when SSI effects are ignored (which is common practice in structural design).

2.1.2 Methodologies for Soil-Structure Interaction Analysis

The general methods by which SSI analyses are performed can be categorized as direct and substructure approaches. In a direct approach, the soil and structure are included within the same model and analyzed in a single step. The soil is often discretized with solid finite elements and the structure with finite beam elements. Because assumptions of superposition are not required, true nonlinear analyses are possible (e.g. Borja et al., 1992 and Weidlinger Assoc., 1978). However, results from

nonlinear analyses can be quite sensitive to poorly-defined parameters in the soil constitutive model, and the analyses remain quite expensive from a computational standpoint. Hence, direct SSI analyses are more commonly performed using equivalent-linear methods to approximate the effects of soil nonlinearity (e.g. FLUSH, Lysmer et al., 1975).

In a substructure approach, the SSI problem is broken down into three distinct parts which are combined to formulate the complete solution. The superposition inherent to this approach requires an assumption of linear soil and structure behavior. Referring to Fig. 2.1, the three steps in the analysis are as follows:

1. Evaluation of a Foundation Input Motion (FIM), which is the motion that would occur on the base-slab if the structure and foundation had no mass. The FIM is dependent on the stiffness and geometry of the foundation and soil. Since inertial effects are neglected, the FIM represents the effects of kinematic interaction only.
2. Determination of the impedance function. The impedance function describes the stiffness and damping characteristics of foundation-soil interaction. It should account for the soil stratigraphy and foundation stiffness and geometry, and is computed using equivalent-linear soil properties appropriate for the in situ dynamic shear strains.
3. Dynamic analysis of the structure supported on a compliant base represented by the impedance function and subjected to a base excitation consisting of the FIM.

The principal advantage of the substructure approach is its flexibility. Because each step is independent of the others, the analyst can focus resources on the most significant aspects of the problem.

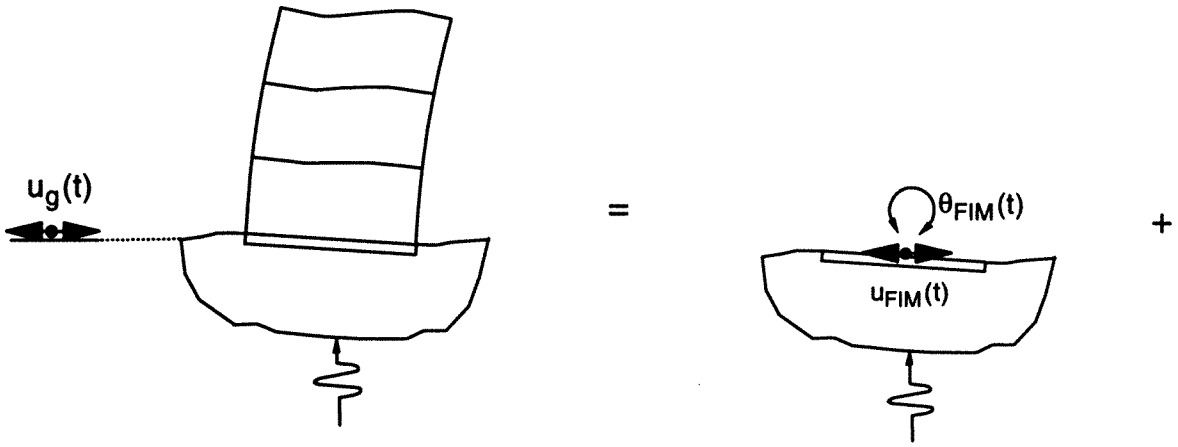

Interaction Problem

(1) Kinematic Interaction,
Evaluation of Foundation Input Motions

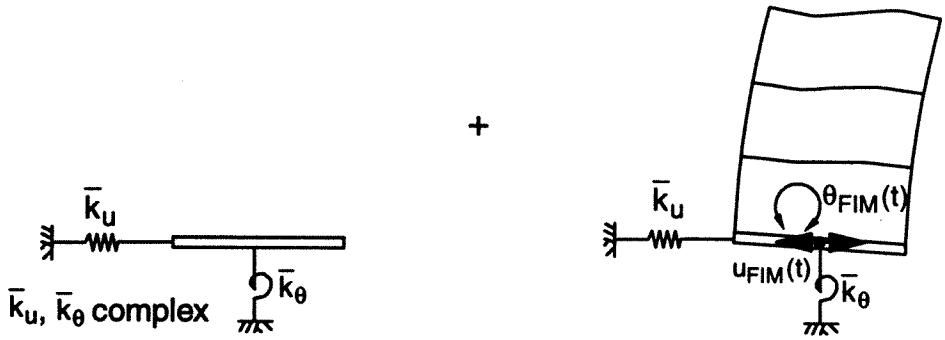

(2) Impedance Function

(3) Analysis of structure on
compliant base subjected to FIM

Fig. 2.1: Substructure approach to analysis of the SSI problem

The simplified analytical formulations which are calibrated in this study against "empirical" data are based on the substructure approach. Analyses of inertial interaction effects predict the variations of first-mode period and damping ratio between the actual "flexible-base" case (which incorporates the flexibility of both the foundation-soil system and the structure) and a fictional "fixed-base" case (which incorporates only the flexibility of the structure). The flexible-base modal parameters can be used with a free-field response spectrum to evaluate design base shear forces for the structure. Hence, these analyses correspond to Steps 2 and 3 of the substructure approach. The analyses for kinematic interaction (Step 1 of the substructure approach) predict frequency-dependent transfer function amplitudes relating foundation and free-field motions.

SSI provisions in the Applied Technology Council (ATC, 1978) and the National Earthquake Hazards Reduction Program (NEHRP) (BSSC, 1997) seismic design codes are similar to portions of the inertial interaction analysis procedures described in this chapter. Kinematic interaction effects are neglected in the code provisions, meaning that free-field motions and FIMs are assumed to be identical.

The literature on SSI analytical techniques is extensive, and it is not the purpose of this chapter to review it comprehensively. Rather, the emphasis is on providing background for the analysis procedures used to predict SSI effects at the sites considered in this study. Inertial and kinematic interaction analyses are discussed in Sections 2.2 and 2.3, respectively.

2.2 Inertial Interaction

2.2.1 System Considered

A system commonly employed in simplified analyses of inertial interaction is shown in Fig. 2.2. The system consists of a single degree-of-freedom structure with height h, mass m, stiffness k, and viscous damping coefficient c. The base of the structure is allowed to translate relative to the free-field an amount u_f and rotate an amount θ. The impedance function is represented by lateral and rotational springs with complex stiffnesses $\bar{k}_u$ and $\bar{k}_\theta$, respectively. The imaginary components of the foundation stiffness terms represent the effects of damping.

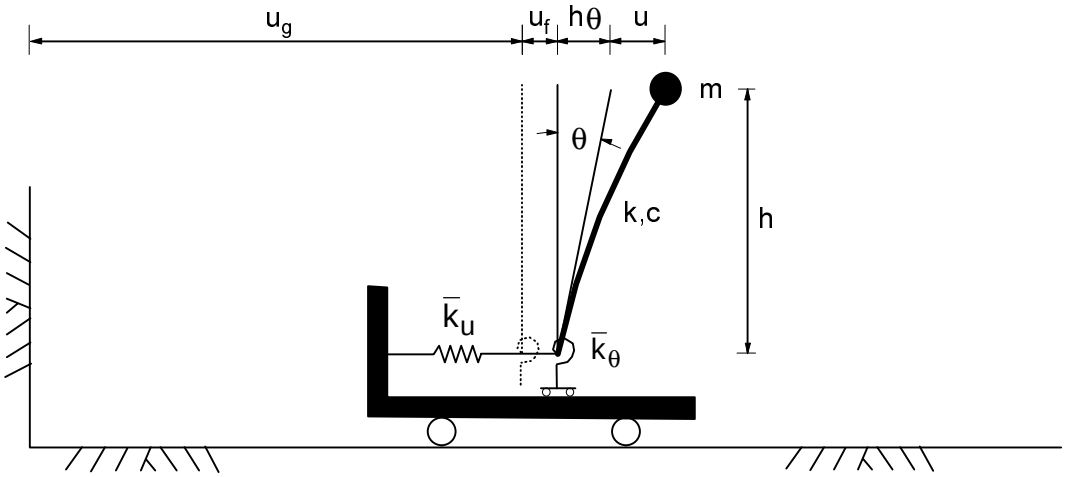

Fig. 2.2: Simplified model for analysis of inertial interaction

The simple system in Fig. 2.2 can be viewed as a direct model of a single-story building or, more generally, as an approximate model of a multi-mode, multi-story structure which is dominated by first-mode response. In the latter case, h is interpreted

as the distance from the base to the centroid of the inertial forces associated with the first vibration mode.

2.2.2 Impedance Function

In general, the impedance function is the most poorly defined component of the model in Fig. 2.2. As described previously, the impedance function represents the dynamic stiffness and damping characteristics of foundation-soil interaction. Mathematically, an impedance function is a matrix which relates the forces (e.g. base shear and moment) at the base of the structure to the displacements and rotations of the foundation relative to the free-field. The terms in the impedance function are complex-valued and frequency dependent. When values of impedance parameters at a single frequency must be used (as is the case for the model in Fig. 2.2), values at the predominant frequency of the soil-structure system are selected.

(a) *Basic case*

In the most general case, six degrees of freedom would be necessary for each support point on the foundation. In practice, however, the foundation is often assumed to be rigid, which reduces the total degrees of freedom to six. When considering the lateral response of a structure on a rigid foundation in a particular direction, as is the case for the model in Fig. 2.2, only two impedance terms are generally necessary (Eq. 2.1). In Eq. 2.1, off-diagonal terms are neglected as they are usually small. It should be noted that vertical excitation and torsion are neglected in the simple impedance function in Eq. 2.1.

$$\begin{bmatrix} V \\ M \end{bmatrix} = \begin{bmatrix} \bar{k}_u & 0 \\ 0 & \bar{k}_\theta \end{bmatrix} \begin{bmatrix} u_f \\ \theta \end{bmatrix} \tag{2.1}$$

A number of analytical procedures are available for the computation of impedance functions, many of which are summarized in Luco (1980b) and Roesset (1980). Perhaps the most widely used solution is that for a rigid circular foundation on the surface of a visco-elastic halfspace (Veletsos and Wei, 1971 and Veletsos and Verbic, 1973). This solution accounts for the three-dimensional nature of the problem and the frequency dependence of the stiffness and damping parameters.

In the solution for a rigid disk on a halfspace, terms in the impedance function are expressed in the form

$$\bar{k}_j = k_j(a_0, \upsilon) + i\omega c_j(a_0, \upsilon) \tag{2.2}$$

where *j* denotes either deformation mode u or θ, ω is angular frequency (radians/sec.), a_0 is a dimensionless frequency defined by $a_0 = \omega r/V_S$, r = foundation radius, V_S = soil shear wave velocity, and υ = soil Poisson ratio. Foundation radii are computed separately for translational and rotational deformation modes to match the area (A_f) and moment of inertia (I_f) of the actual foundation, as follows,

$$r_1 = \sqrt{\frac{A_f}{\pi}} \qquad r_2 = \sqrt[4]{\frac{4 \cdot I_f}{\pi}} \tag{2.3}$$

There are corresponding different values of $(a_0)_1$ and $(a_0)_2$ as well.

The real stiffness and damping of the translational and rotational springs and dashpots are expressed, respectively, by

$$k_u = \alpha_u K_u \tag{2.4a}$$

$$c_u = \beta_u \frac{K_u r_1}{V_S} \tag{2.4b}$$

$$k_\theta = \alpha_\theta K_\theta \tag{2.4c}$$

$$c_\theta = \beta_\theta \frac{K_\theta r_2}{V_S} \tag{2.4d}$$

The quantities α_u, β_u, α_θ, and β_θ are dimensionless parameters expressing the frequency dependence of the results, while K_u and K_θ represent the static stiffness of a disk on a halfspace, defined by

$$K_u = \frac{8}{2-\upsilon} G r_1 \tag{2.5a}$$

$$K_\theta = \frac{8}{3(1-\upsilon)} G r_2^3 \tag{2.5b}$$

where G = soil dynamic shear modulus. Presented in Fig. 2.3 are the frequency-dependent values of α_u, β_u, α_θ, and β_θ for $\upsilon = 0.4$ based on closed form expressions in Veletsos and Verbic (1973). These results are similar to those obtained by Luco and Westmann (1971) for the case of a circular foundation on the surface of an elastic halfspace.

Values of soil shear stiffness G and hysteretic damping β used in the formulation of impedance functions should be appropriate for the in situ shear strains. For this study, these parameters were established from deconvolution analyses performed with the one-dimensional site response program SHAKE (Schnabel et al., 1972). In these analyses, nonlinear soil behavior is simulated by the equivalent-linear technique. Details on soil modeling and profile depths used in these analyses are provided in Stewart (1997). When

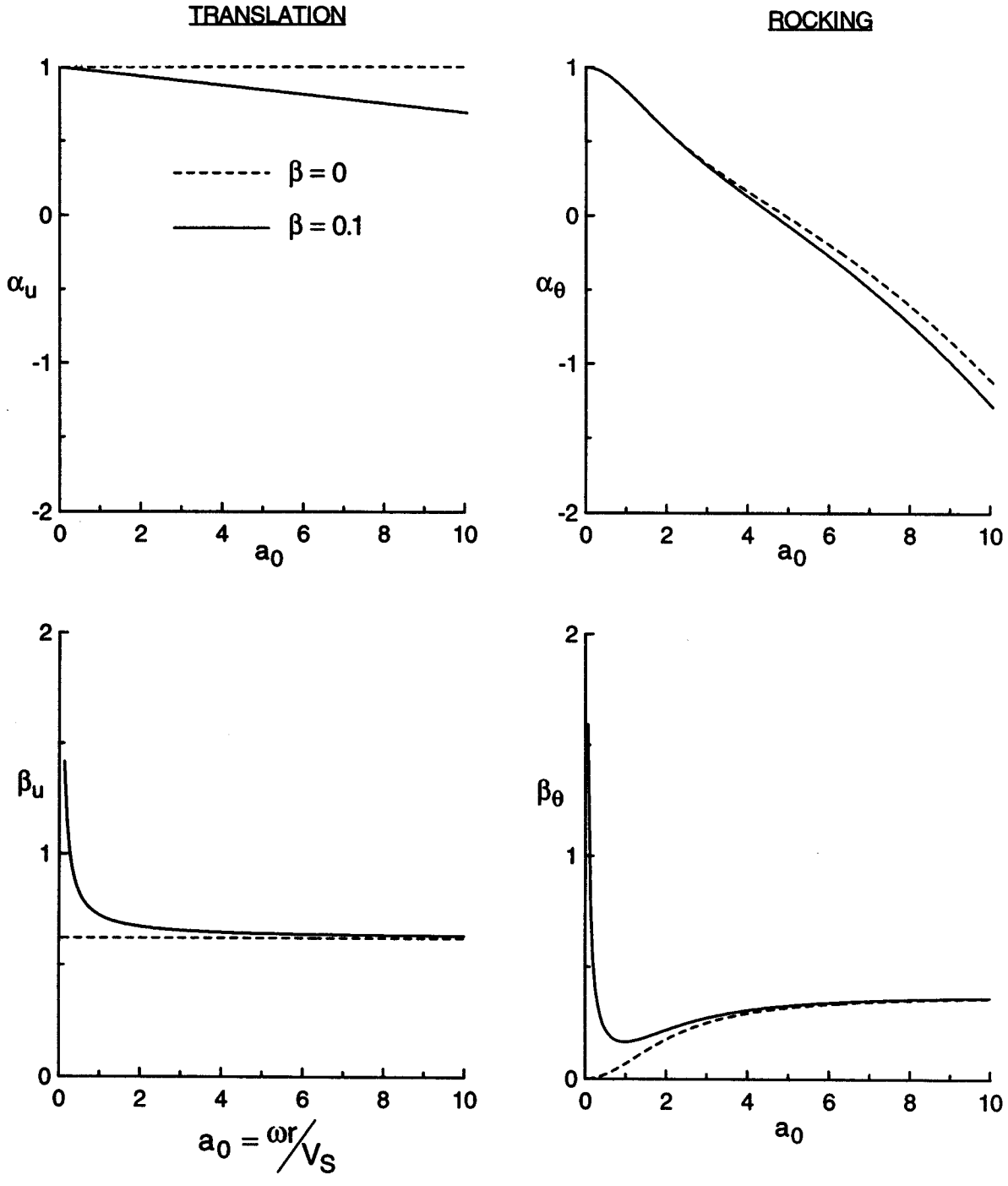

Fig. 2.3: Foundation stiffness and damping factors for elastic and viscoelastic halfspaces, $\upsilon = 0.4$ (after Veletsos and Verbic, 1973)

compared to recorded motions, results obtained from SHAKE deconvolution analyses have generally been well verified at shallow depths (i.e. 50 to 100 feet, e.g. Chang et al., 1985 and Geomatrix, 1991). Although shear strains resulting from SSI are not modeled by these deconvolution analyses, such strains are generally small relative to the strains associated with the free-field ground response.

Validation studies for the above and similar impedance function formulations have been conducted by Lin and Jennings (1984) and Crouse et al. (1990) for small surface foundations. In the Lin and Jennings study, a 10 x 10-foot specimen structure was subjected to sinusoidal ground vibrations generated in an excitation structure located about 50 feet away. The foundation impedance at the resonant frequency of the specimen structure was derived from the experimental results, and was consistent with theoretical predictions by Veletsos and Wei (1971). In the Crouse et al. (1990) study, two 4 x 4-foot slabs (one founded essentially at the ground surface and the other having 1.5 to 2.0-foot deep piers at the corners) were subjected to sinusoidal forced vibration testing across a range of frequencies from 10 to 60 Hz with a shaker mounted on the slabs. Impedance functions evaluated from these test results were compared to theoretical functions for layered media derived from integral equations (Apsel and Luco, 1987). The experimental and theoretical frequency-dependent impedances agreed reasonably well given the uncertainty in near-surface V_S data at the two sites, though the agreement was considerably better for the slab without corner piers. Theoretical results from Apsel and Luco (1987) and Veletsos and Verbic (1973) are nearly identical for surface foundations, hence these experimental results effectively validate both formulations.

Despite the demonstrated utility of the impedance function formulation by Veletsos and Verbic, commonly encountered conditions such as nonuniform soil profiles, embedded, non-circular, or flexible foundations, and the presence of piles or piers are not directly modeled by these procedures. The effects of such conditions (except piles or piers) on foundation impedance can be approximately simulated with adjustments to the basic solution, as discussed in Parts (b) through (e) below.

(b) *Nonuniform soil profiles*

Nonuniform soil profiles can often be characterized by gradual increases in stiffness with depth, or by a very stiff layer underlying relatively soft, surficial layers. For profiles having gradual increases in stiffness with depth, Roesset (1980) found that using soil properties from a depth of about $0.5 \cdot r$ gave halfspace impedances which reasonably simulated the impedance of the variable profile. In this study, equivalent halfspace velocities were computed as $V_S = r_1/t_{r\text{-}0}$, where $t_{r\text{-}0}$ is the travel time for vertically propagating shear waves to travel from a depth r_1 to the ground surface. These equivalent halfspace velocities are often similar to the actual V_S at a depth of $0.5 \cdot r_1$. Details on the calculation of V_S for individual sites are presented in Stewart (1997).

For the case of a finite soil layer overlying a much stiffer material, the key considerations are an increase in the static stiffness and changes in the frequency dependent variations of stiffness and damping. The increased static stiffnesses can be estimated as follows (Kausel, 1974),

$$(K_u)_{FL} = K_u\left(1+\frac{1}{2}\frac{r_1}{d_s}\right)$$
$$(K_\theta)_{FL} = K_\theta\left(1+\frac{1}{6}\frac{r_2}{d_s}\right) \qquad (2.6)$$

where $(K_u)_{FL}$ and $(K_\theta)_{FL}$ are the static horizontal and rocking stiffnesses of the foundation on finite soil layer, and d_S is the depth of the layer. The frequency dependent variations of stiffness terms follow the general trends for a halfspace in Fig. 2.3, but have oscillations associated with the natural frequency of the stratum at low levels of soil damping. For hysteretic damping exceeding about 7%, Roesset (1980) found that the oscillations can be neglected. With regard to damping, the key issue is a lack of radiation damping at frequencies less than the fundamental frequency of the finite soil layer. Halfspace damping ratios can be used for frequencies greater than the soil layer frequency, and a transition to zero radiation damping at smaller frequencies can be defined per Elsabee and Morray (1977).

(c) *Foundation embedment*

Foundation embedment effects were investigated by Elsabee and Morray (1977) for the case of a circular foundation embedded to a depth e into a homogeneous soil layer of depth d_S (Fig. 2.4). It was found that the static horizontal and rocking stiffness for such foundations [$(K_U)_{FL/E}$ and $(K_\theta)_{FL/E}$] is approximated as follows for $r/d_S < 0.5$ and $e/r < 1$:

$$(K_u)_{FL/E} = K_u\left(1+\frac{2}{3}\frac{e}{r}\right)\left(1+\frac{5}{4}\frac{e}{d_s}\right)\left(1+\frac{1}{2}\frac{r}{d_s}\right)$$
$$(K_\theta)_{FL/E} = K_\theta\left(1+2\frac{e}{r}\right)\left(1+0.7\frac{e}{d_s}\right)\left(1+\frac{1}{6}\frac{r}{d_s}\right) \qquad (2.7)$$

Coupling impedance terms were found to be small relative to $(K_u)_{FL/E}$ and $(K_\theta)_{FL/E}$ for small embedment ratios (i.e. e/r < 0.5). Elsabee and Morray suggested that the frequency dependence of the foundation stiffness and damping terms could be approximated as per Eqs. 2.4a-d (which strictly apply only for a rigid, circular surface foundation on a halfspace). These recommendations have been adopted into the NEHRP (BSSC, 1997) code provisions, with the exception of the frequency dependence stiffness terms (α) which are assumed to be unity.

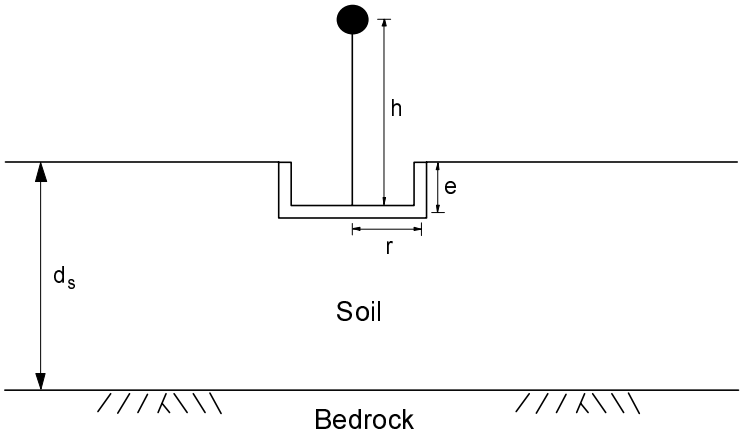

Fig. 2.4: Embedded soil-foundation-structure system on finite soil layer

Approximate normalized impedance factors for a cylindrical foundation embedded in a halfspace obtained from Eq. 2.7 are compared to a more rigorous analytical solution derived from integral equations (Apsel and Luco, 1987) in Fig. 2.5. The approximate curves were computed as the product of dimensionless impedance factors α_u, α_θ, β_u, and β_θ and the first modifier on the right hand side of Eq. 2.7. Both solutions apply for a uniform visco-elastic halfspace with β=1%, ν = 0.25, and perfect bonding between the soil and foundation. The comparisons are generally poor, with the exception of stiffness

terms α_u and α_θ, which are reasonably well predicted for $e/r \leq 0.5$, and in the case of α_θ, for $a_0 < 1.5$ as well. In the case of damping, the comparison in Fig. 2.5 is essentially one of radiation damping effects due to the low β value in this example. The approximation grossly underpredicts radiation damping effects even at moderate embedments (e.g. $e/r = 0.5$) at all frequencies. However, this underprediction of radiation damping may be tolerable in some situations, because at the low frequencies typical of many structures ($a_0<1$), radiation damping effects are small relative to hysteretic soil damping, and consequently estimates of total foundation damping may be reasonable.

Field vibration testing of a small (10 x 10 ft) embedded structure (Lin and Jennings, 1984) found that Elsabee and Morray's predictions of the embedment effect on rocking stiffness and damping were fairly accurate, especially for low embedment ratios ($e/r = 0.44$). However, translational stiffness and damping were significantly underpredicted for both embedment ratios tested (0.44 and 0.90). Forced vibration testing of a nine-story reinforced concrete building with a single-level basement ($e/r = 13/45$ ft $= 0.29$) by Wong et al. (1988) revealed low frequency ($a_0 \approx 0.2$ to 0.4) impedance function ordinates for rocking that were in excellent agreement with the Apsel and Luco theoretical predictions (and, by inference, the approximate solution as well). Horizontal stiffness was found to be overpredicted by the Apsel and Luco theory by about 20 to 40%, while damping comparisons were inconclusive.

In this study, embedment effects on foundation impedance were evaluated with two separate analyses. The first analysis is based on static foundation stiffnesses established per Eq. 2.7 (with coupling terms assumed to be zero) and frequency dependent modifications to stiffness and damping terms with the α_u, α_θ, β_u, and β_θ factors in Eq.

2.4a-d. The second analysis, formulated by Bielak (1975), more rigorously incorporates soil/basement-wall interaction effects into the foundation impedance function, and hence is similar to Apsel and Luco (1987). This second formulation is discussed further in Section 2.2.3.

(d) *Foundation shape*

Conventional practice has been that foundations of arbitrary shape are analyzed as equivalent circular mats, provided that the foundation aspect ratio in plan (L/B) is less than 4:1 (Roesset, 1980). As noted in Eq. 2.3, an equivalent radius for translational stiffness is derived by equating the area of the mats, while an equivalent radius for rocking stiffness is derived by equating the moment of inertia of the mats. These criteria have been adopted into the NEHRP (BSSC, 1997) code.

Dobry and Gazetas (1986) reviewed the literature for impedance function solutions for foundations of various shapes including circles and rectangles with aspect ratios of 1 to ∞. Their results generally confirmed that the use of equivalent circular mats is an acceptable practice for aspect ratios < 4:1, with the notable exception of dashpot coefficients in the rocking mode. As shown in Fig. 2.6, dimensionless radiation damping coefficients c_{rx} and c_{ry} (for longitudinal and transverse rocking, respectively) are seen to be underestimated by the equivalent disk assumption at low frequencies. This is a consequence of the tendency for rocking vibrations to be dissipated into the soil primarily via the ends of the foundation. Hence, as L/B increases, the two ends act increasingly as independent wave sources with reduced destructive interference between waves emanating from the foundation. For the case of longitudinal rocking, damping can be

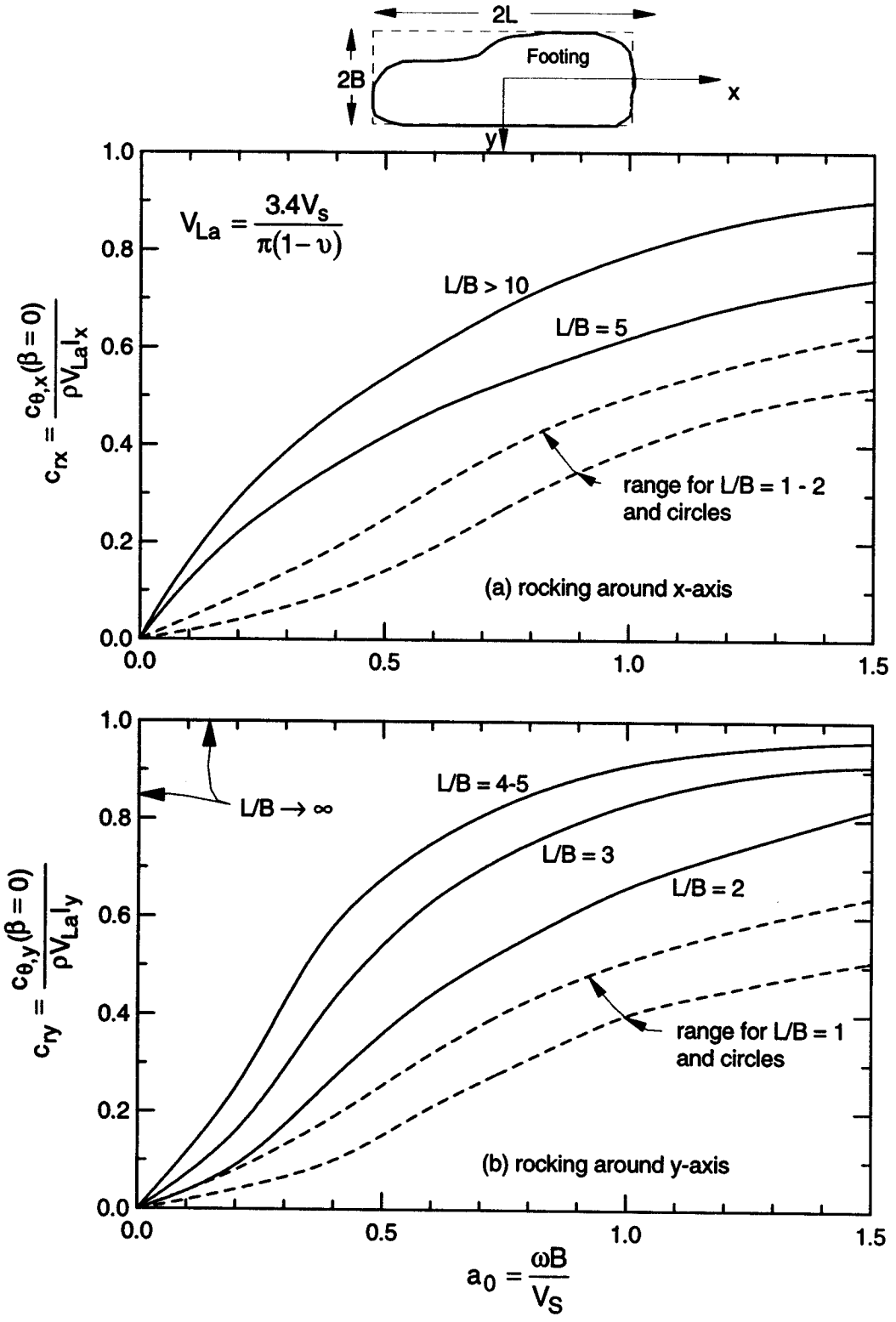

Fig. 2.6: Dashpot coefficients for rocking radiation damping vs. frequency for different foundation shapes (Dobry and Gazetas, 1986)

underpredicted by more than 100% for aspect ratios of L/B ≈ 4. For higher frequencies (a_0 > 3 - 4, not shown), the results for the various aspect ratios converge to c_{rx}, c_{ry} ~ 1. This occurs because these high frequency waves have short wavelengths, so destructive interference between the waves decreases.

In this study, radiation dashpot coefficients for oblong, non-circular foundations were corrected according to the results in Fig. 2.6. This correction was made by multiplying the radiation damping component of the disk dashpot coefficients from Part (a) by $(c_r)_{L/B}/(c_r)_{L/B=1}$, where the c_r values were determined at the a_0 value corresponding to the structure's fundamental frequency.

(e) *Foundation flexibility*

The effects of foundation flexibility on impedance functions for surface disk foundations have been investigated by Iguchi and Luco (1982) for the case of loading applied through a rigid central core, Liou and Huang (1994) for the case of thin perimeter walls, and Riggs and Waas (1985) for the case of rigid concentric walls (Fig. 2.7). These studies have generally focused on foundation flexibility effects on rocking impedance; the horizontal impedance of non-rigid and rigid foundations are similar (Liou and Huang, 1994).

A key parameter in the evaluation of foundation flexibility effects on rocking impedance is the ratio of the soil-to-foundation rigidity,

$$\eta = \frac{Gr^3}{D} \tag{2.8}$$

in which G is the soil dynamic shear modulus and D is the foundation's flexural rigidity,

$$D = \frac{E_f t_f^3}{12\left(1-\upsilon_f^2\right)} \tag{2.9}$$

where E_f, t_f, and ν_f are the Young's modulus, thickness, and Poisson's ratio of the foundation, respectively. For the case of rocking impedance, the significance of foundation flexibility effects depends on the wall configuration on the disk. As shown in Fig. 2.8, these effects are most important for the rigid central core case, for which significant reductions in stiffness and damping are possible. The reductions are greatest for narrow central cores and large values of relative soil/foundation rigidity (i.e. η = 10 to 1000). For the case of thin perimeter walls, the foundation impedances are reasonably close to rigid base values for $a_0 < 3$. For the concentric wall case considered by Riggs and Waas (1985), it was similarly found that flexible foundations behave similarly to rigid foundations at low frequencies.

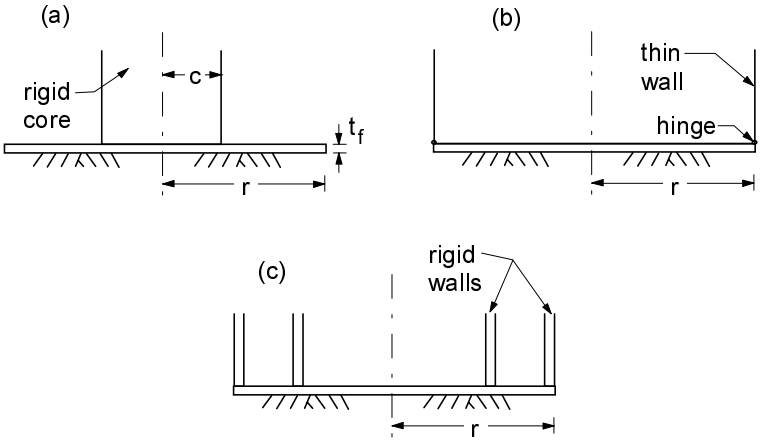

Fig. 2.7: Disk foundations with (a) rigid core considered by Iguchi and Luco (1982) (b) thin perimeter walls considered by Liou and Huang (1994), and (c) rigid concentric walls considered by Riggs and Waas (1985)

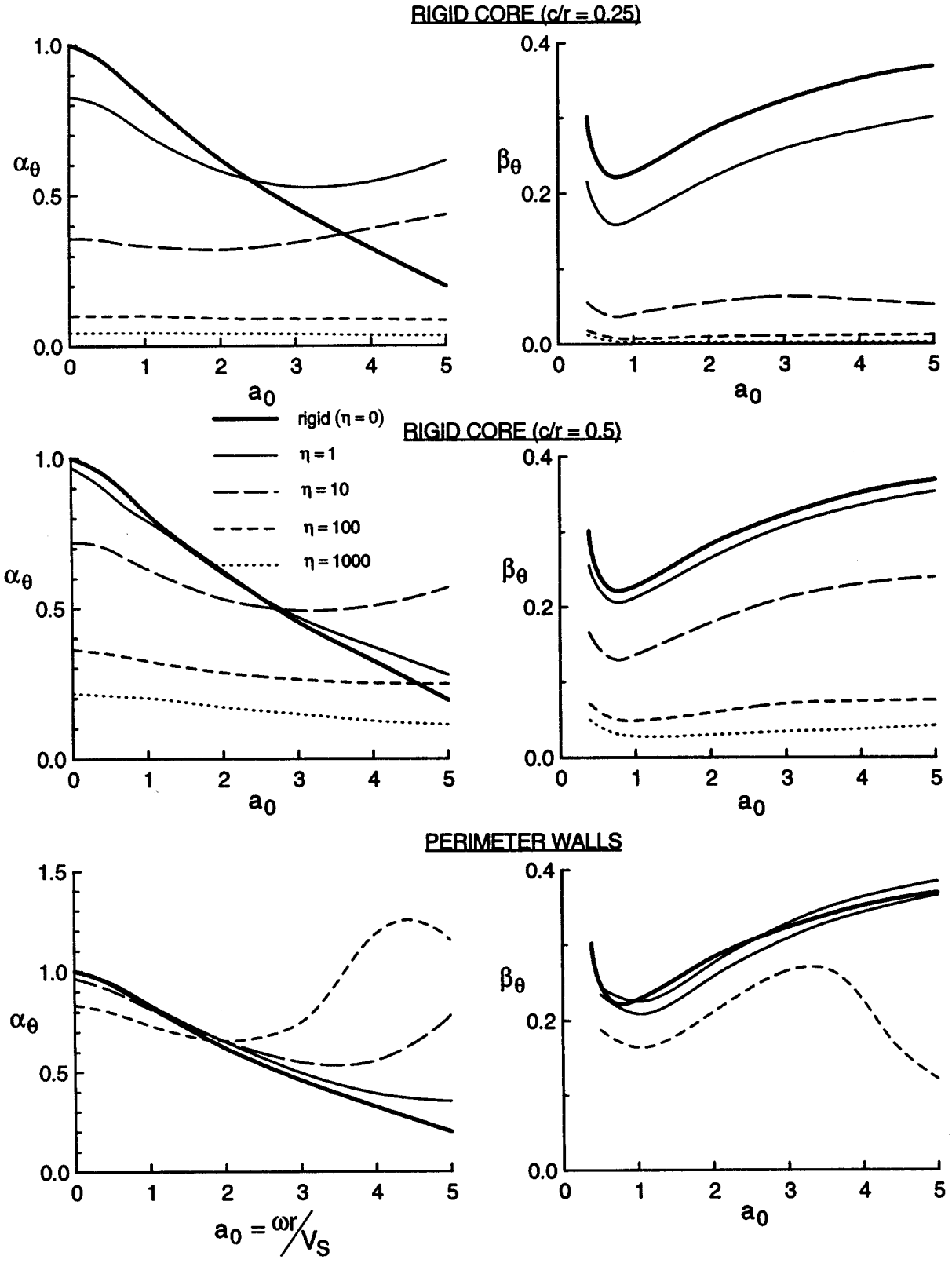

Fig. 2.8: Rocking stiffness and damping factors for flexible foundations; rigid core cases (Iguchi and Luco, 1982) and perimeter wall case (Liou and Huang, 1994)

In this study, corrections for foundation flexibility effects were made to rocking impedance terms for structures having central core shear walls using the curves in Fig. 2.8. This correction was made by multiplying the disk rocking stiffness and dashpot coefficients from Part (a) by $(\alpha_\theta)_{flex}/(\alpha_\theta)_{rigid}$ and $(\beta_\theta)_{flex}/(\beta_\theta)_{rigid}$, respectively, where the α_θ and β_θ values were determined at the a_0 value corresponding to the structure frequency. No corrections to rocking impedance terms were made for other wall configurations, nor were corrections applied to horizontal impedance terms.

(f) *Piles or piers*

The influence of pile foundations on impedance functions cannot easily be accounted for with simplified analyses. Many analytical techniques are available for evaluating the impedance of pile supported foundations (e.g. Novak, 1991 and Gohl, 1993), but a review of such techniques is beyond the scope of this chapter. The effects of piles/piers were not explicitly accounted for in the development of impedance functions for the analyses in this study. Instead, the influence of foundation type on the final results was evaluated empirically, as discussed in Chapter 5.

2.2.3 Results

Veletsos and Meek (1974) found that the maximum seismically induced deformations of the oscillator in Fig. 2.2 could be predicted accurately by an equivalent fixed-base single degree-of-freedom oscillator with period $\tilde{T}$ and damping ratio $\tilde{\zeta}$. These are referred to as “flexible-base” parameters, as they represent the properties of an

oscillator which is allowed to translate and rotate at its base (i.e. Fig. 2.2). The flexible-base period is evaluated from (Veletsos and Meek, 1974),

$$\frac{\tilde{T}}{T} = \sqrt{1 + \frac{k}{k_u} + \frac{kh^2}{k_\theta}} \tag{2.10}$$

where T is the fixed-base period of the oscillator in Fig. 2.2 (i.e. the period that would occur in the absence of base translation or rocking). The flexible-base damping ratio has contributions from the viscous damping in the structure as well as radiation and hysteretic damping in the foundation. Jennings and Bielak (1973) and Veletsos and Nair (1975) expressed the flexible-base damping $\tilde{\zeta}$ as

$$\tilde{\zeta} = \tilde{\zeta}_0 + \frac{\zeta}{\left(\tilde{T}/T\right)^3} \tag{2.11}$$

where $\tilde{\zeta}_0$ is referred to as the foundation damping factor and represents the damping contributions from foundation-soil interaction (with hysteretic and radiation components). A closed form expression for $\tilde{\zeta}_0$ is presented in Veletsos and Nair (1975).

The relationships between the fixed- and flexible-base oscillator properties depend on aspect ratio h/r_2, soil Poisson Ratio υ, soil hysteretic damping ratio β, and the following dimensionless parameters:

$$\sigma = V_S T/h \tag{2.12}$$

$$\gamma = \frac{m}{\rho \pi r_1^2 h} \tag{2.13}$$

Parameters σ and γ represent the ratio of the soil-to-structure stiffness and structure-to-soil mass, respectively. For conventional building structures, $\sigma > 2$ and $\gamma \approx 0.1$ to 0.2 [a

representative value of $\gamma = 0.15$ is recommended by Veletsos and Meek (1974)]. Both $\tilde{T}/T$ and $\tilde{\zeta}_0$ are sensitive to σ, while the sensitivity to γ is modest for $\tilde{T}/T$ ($\pm$ 10 to 15% error), and low for $\tilde{\zeta}_0$ (Aviles and Perez-Rocha, 1996).

For the case of a rigid circular foundation on the surface of a visco-elastic halfspace (impedance defined in Section 2.2.2), analytical results from Veletsos and Nair (1975) for $\tilde{T}/T$ and $\tilde{\zeta}_0$ vs. $1/\sigma$ are shown in Figs. 2.9 and 2.10, respectively. The results show that $\tilde{T}$ is always lengthened relative to T, and that the period lengthening ratio ($\tilde{T}/T$) increases with $1/\sigma$ and h/r for $h/r > 1$. This implies that the ratio of structure-to-soil stiffness ($1/\sigma$) is a critical factor controlling the period lengthening, and that for a given value of $1/\sigma$, period lengthening increases for taller structures (i.e. higher h/r) with more overturning moment. The flexible base damping $\tilde{\zeta}$ can actually increase or decrease relative to ζ depending on the period lengthening in the structure and the foundation damping factor $\tilde{\zeta}_0$. In Fig. 2.10, $\tilde{\zeta}_0$ is seen to increase with $1/\sigma$ and decrease with h/r, indicating that lateral movements of the foundation (which dominate at low h/r) dissipate energy into soil more efficiently than foundation rocking (which dominates at high h/r). The contributions to foundation damping from radiation and hysteretic damping are compared in Fig. 2.10; the significance of hysteretic damping is seen to increase with increasing h/r due to the decreased radiation damping effect.

For the case of a rigid circular foundation embedded into a visco-elastic soil, analytical results for $\tilde{T}/T$ and $\tilde{\zeta}_0$ vs. $1/\sigma$ are shown in Fig. 2.11 for the analytical formulation presented above (i.e. the Veletsos and Nair (V & N) model) as well as two

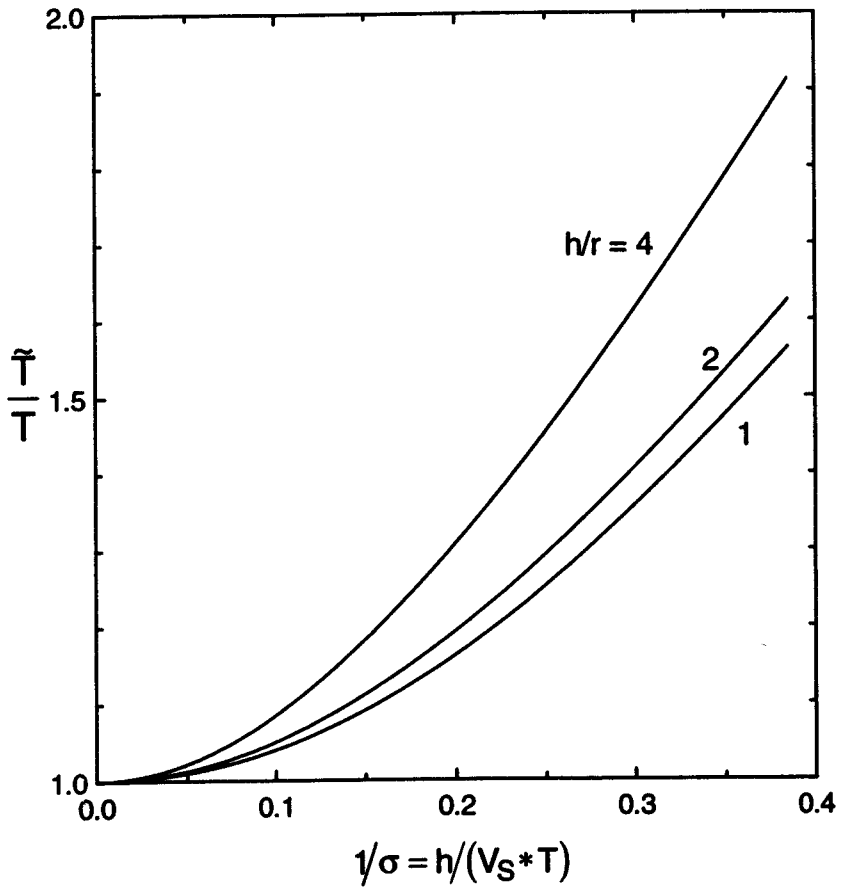

Fig. 2.9: Period lengthening ratios for single degree-of-freedom structure with rigid circular foundation on viscoelastic halfspace ($\upsilon = 0.4, \gamma = 0.15$) [Veletsos and Nair, 1975]

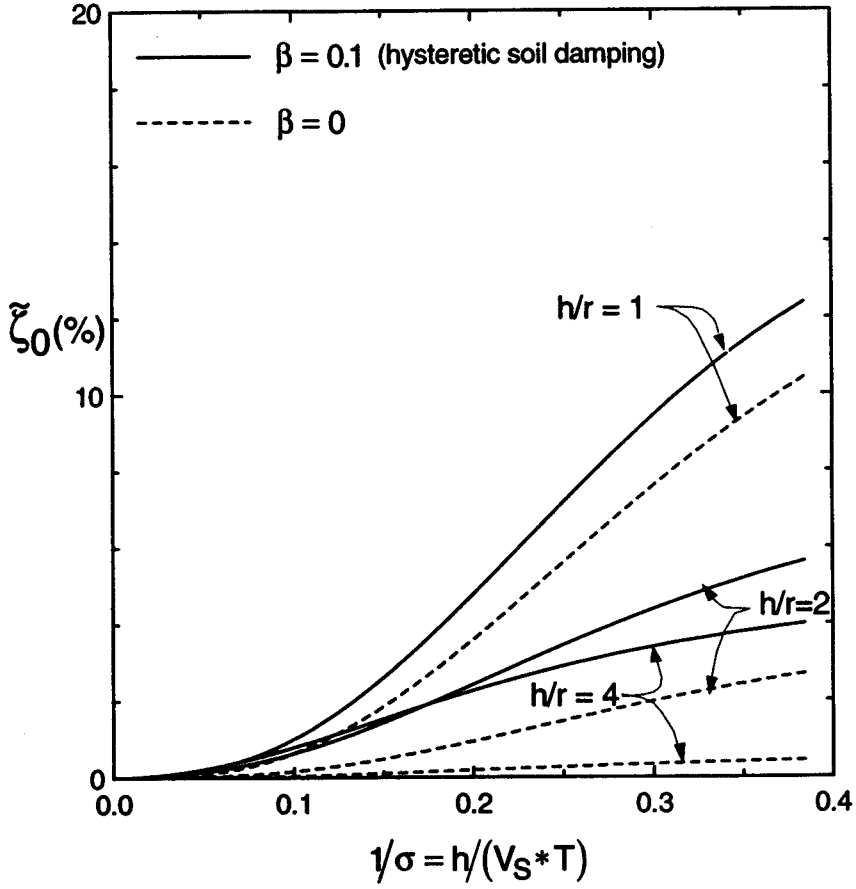

Fig. 2.10: Foundation damping factors for single degree-of-freedom structure with rigid circular foundation on elastic and viscoelastic half-space ($\upsilon = 0.4, \gamma = 0.15$) [Veletsos and Nair, 1975]

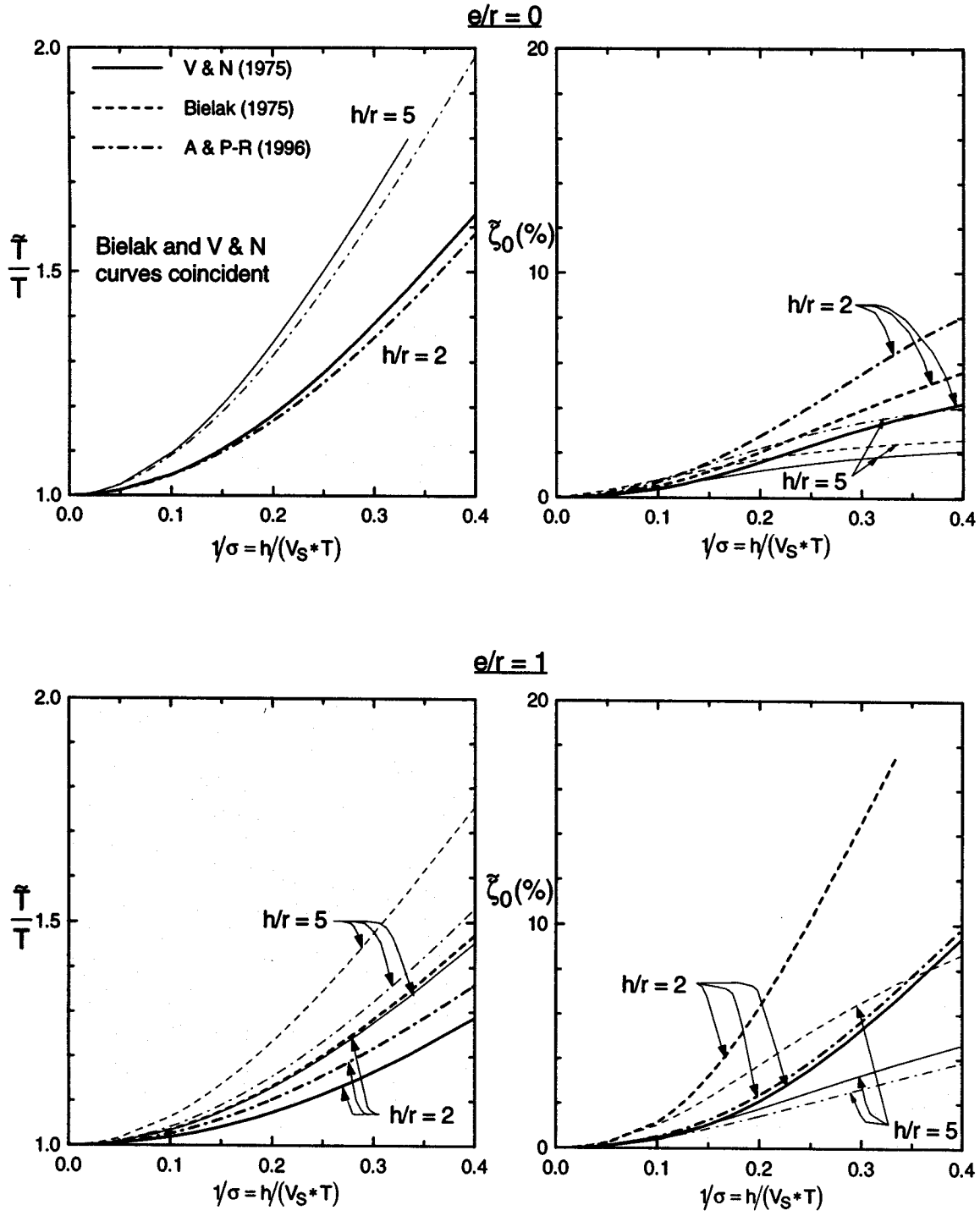

Fig. 2.11: Comparison of period lengthening ratios and foundation damping factors for single degree-of-freedom structure with surface and embedded foundations ($\upsilon = 0.45, \beta = 5\%, \gamma = 0.15, \zeta = 5\%$)
[Veletsos and Nair, 1975; Bielak, 1975; Aviles and Perez-Rocha, 1996]

others [Bielak (1975) and Aviles and Perez-Rocha (A & P-R), 1996]. The V & N and Bielak solutions are for a foundation embedded into a halfspace, while the A & P-R solution is for a thick finite layer ($d_S/r = 10$). The SSI models solved in the Bielak and V & N approaches are similar, except that dynamic soil/basement-wall interaction effects on foundation impedance are incorporated into the Bielak formulation. Similarly, the only significant difference between the A & P-R and Bielak models is the finite soil layer used by A & P-R. For the plots in Fig. 2.11, embedment corrections for the V & N approach were made according to Eq. 2.7. For the case of zero embedment ($e/r = 0$), the three formulations yield essentially identical results with the exception of relatively high damping from the A & P-R model. For the case of $e/r = 1$, increases in damping and decreases in period lengthening are predicted by all three models. The Bielak model yields the highest damping predictions. V & N and A & P-R indicate smaller damping due to the lack of a dynamic basement wall-soil interaction model (V & N) and the finite soil layer (A & P-R). It should be noted that the embedment ratio $e/r = 1$ is approaching the limit of validity for the expression in Eq. 2.7, and results from the three formulations are more consistent for lower e/r.

In this study, the analysis by Veletsos and Nair (1975) was generally used with appropriate modifications to the foundation impedance for nonuniform soil profiles, foundation embedment (i.e. Eq. 2.7), foundation shape, and foundation flexibility effects. To more accurately model the stiffness and damping of embedded foundations, analyses were also performed using the Bielak (1975) approach with appropriate modifications for nonuniform soil profiles and foundation shape and flexibility effects. For subsequent

reference, these analyses are termed the “modified Veletsos” and “modified Bielak” formulations.

2.2.4 Calibration of Analysis Results with Field Performance Data

Research efforts have been undertaken to calibrate analytical techniques for SSI using seismic field performance data from the Humboldt Bay Nuclear Power Plant (Valera et al., 1977) and the Lotung 1/4-scale containment model (Bechtel Power Corporation, 1991). Several test structures have also been examined by Japanese researchers (e.g. a 12.5 m tower, Ganev et al., 1994, and a 31 m scaled containment structure, Hanada et al., 1988). The objectives of these studies were generally to compare recorded structural motions with predicted analytical motions.

The instrumented structure at the Humboldt site essentially consists of a deep caisson (there is no significant above-ground structure), so the simplified analytical techniques discussed above are not applicable. Fixed- and flexible-base structural periods and damping ratios were evaluated for the Lotung site, though these parameters were not compared to analytical predictions of $\tilde{T}/T$ and $\tilde{\zeta}_0$. However, relatively sophisticated analyses of the soil-structure system using the SASSI (Lysmer et al., 1981) and CLASSI (Luco, 1980b) programs were successful at reasonably accurately reproducing the overall structural response, and hence by inference the flexible-base modal parameters. The analytical formulation in the CLASSI program is based on a substructure procedure similar to that outlined in this section. The accuracy of the CLASSI analyses relative to the Lotung data reinforces the validity of these substructure procedures. Similar confirmation of simple SSI models was obtained in back-analyses of data from the

Japanese test structures. It should be noted that the Humboldt and Lotung sites were included in this study as sites A3 and A46. Data from the Japanese sites could not be obtained for this study.

A number of studies have developed two- or three-dimensional frame models of instrumented structures, verified the model's accuracy using periods identified from recorded data, and investigated SSI effects by varying the base fixity condition (e.g. Wallace and Moehle, 1990 and Fenves and Serino, 1992). The study by Wallace and Moehle examined the response of a 22-story shear wall building in Chilé under forced vibration testing, low-level (0.05g) earthquake shaking, and moderate-level (0.18g) shaking. From three-dimensional frame analyses, the period lengthening was found to be 15%, 22%, and 43% in the forced vibration and earthquake shaking conditions, respectively. For the moderate-level shaking condition, the ATC (1978) procedure predicted 37% period lengthening, which is in good agreement with the 43% from frame analyses. Comparisons were not made for the lower-level shaking conditions. Fenves and Serino examined the response of a 14-story concrete-frame warehouse structure (site A29 in this study) during the 1987 Whittier Earthquake. Fixed-base periods were not reported, but changes in base shear resulting from SSI effects were found to be reasonably predicted by the ATC procedure (using smoothed free-field spectra).

Poland et al. (1994) analyzed the effects of SSI on base shear in four buildings using two simple analytical techniques (FLUSH and ATC code provisions) and compared these results to reductions in the base shear calculated using a single degree-of-freedom structural model subjected to recorded free-field and foundation motions (so-called "time history" analyses). Poor agreement between the analytical and "time history" results was

found. However, it is not clear how to interpret these results as the modal parameters used in the "time history" analyses are not reported. SSI effects on structural response can be more rationally assessed by comparing fixed- and flexible-base modal parameters. It should be noted that the four buildings studied by Poland et al. are also examined in this study (sites A6, A10, A12, and A29).

In addition to the above research efforts, a number of calibration studies for impedance functions have been performed (see Section 2.2.2), and modal parameters of several structures have been evaluated using various system identification techniques with some inferences made about SSI effects (see Stewart, 1997 for references). However, fixed- and flexible-base modal parameters were seldom directly compared in these studies.

It appears that no previous studies have attempted to evaluate on a large scale the fixed- and flexible-base modal parameters of structures subjected to significant levels of seismic excitation for the purpose of calibrating simplified analytical procedures such as those in the ATC and NEHRP codes. This is the principle objective of this study.

2.3 Kinematic Interaction

As noted in Section 2.1, kinematic interaction generally results from base-slab averaging, deconvolution/embedment effects, and wave scattering effects. At present, relatively little is known about the effects of wave scattering on base-slab motions, as its effects are almost invariably combined with more significant base-slab averaging and embedment effects, which are the focus of this section.

2.3.1 Base-Slab Averaging

For vertically incident, coherent wave fields, the motion of a rigid surface foundation is identical to the free-field motion. Base-slab averaging effects result from wave fields which have an angle of incidence relative to the vertical, α_V, or which are incoherent in time and space. Incoherence of seismic waves results from different wave ray paths (i.e. due to laterally traveling seismic waves in the underlying bedrock) and local heterogeneities in the geologic media through which the seismic waves have traveled.

In the presence of incoherent or non-vertically incident wave fields, translational base-slab motions are reduced relative to the free-field, and torsional rotation of the base-slab is introduced. Rocking of the base-slab can also occur in the presence of inclined SV or P waves, but is negligible for SH waves. The reduction of base-slab translation, and the introduction of torsion and rocking, are all effects which tend to become more significant with increasing frequency. The frequency-dependence of these effects is primarily associated with the increased effective size of the foundation relative to the seismic wavelengths at higher frequencies. In addition, incoherence effects are greater at higher frequencies.

Veletsos and Prasad (1989) and Veletsos et al. (1997) evaluated the response of a rigid, massless disk of radius r and a rectangle of dimension 2a by 2b on the surface of an elastic halfspace to incoherent SH waves propagating either vertically or at an angle α_V to the vertical (Fig. 2.12). The incident motions are assumed to be polarized in the x-direction, and the effective horizontal propagation of inclined waves is in the y-direction. A result of the analyses is transfer functions relating the horizontal and torsional motions

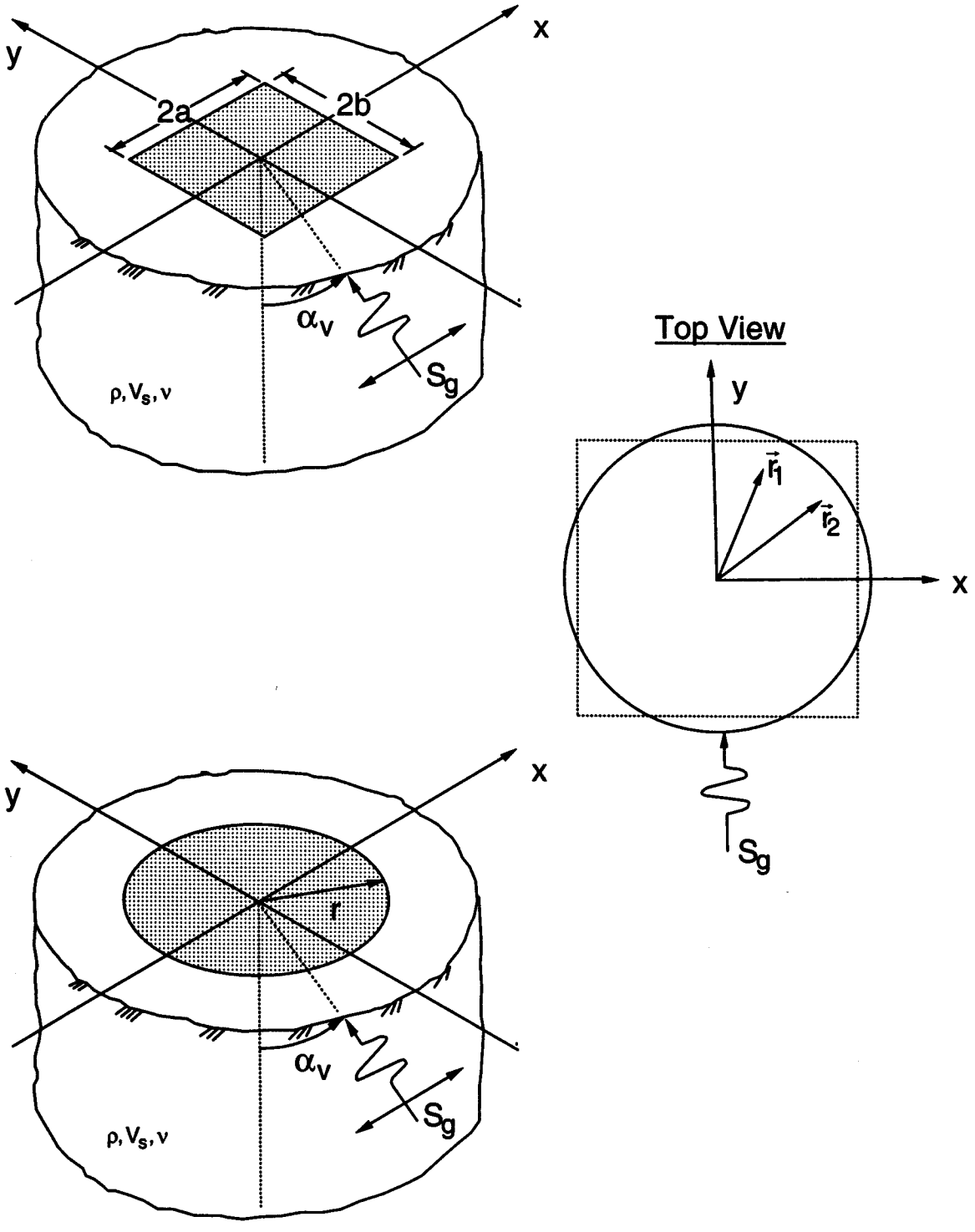

Fig. 2.12: System considered for kinematic interaction analyses (Veletsos and Prasad, 1989 and Veletsos et al., 1997)

of the foundation to the free-field motions, thus providing a quantification of base-slab averaging effects. Similar analytical formulations were developed by Luco and Wong (1986) for rectangular foundations and Luco and Mita (1987) for circular foundations. The Veletsos approach is presented here because of the relative simplicity of its formulation.

A key step in the development of the transfer functions is the numerical modeling of the spatial variation of the free-field ground motions. The temporal variation of these motions is specified by a space invariant power spectral density (psd) function, $S_g(\omega)$. The spatial variation of the incoherent free-field motions is defined by a cross spectral density function,

$$S_{xy}(\omega) = \Gamma\left(|\mathbf{r}_1 - \mathbf{r}_2|, \omega\right) e^{-\left(\frac{i\omega}{(V_S)_H}|\mathbf{r}_1 - \mathbf{r}_2|\right)} S_g(\omega) \tag{2.14}$$

where $\mathbf{r}_1$ and $\mathbf{r}_2$ are position vectors for two points, and $(V_S)_H$ is the apparent horizontal velocity of the wave front, $(V_S)_H = V_S/\sin\alpha_V$. In Eq. 2.14, the exponential term represents the wave passage effect (due to nonvertically incident waves), and the Γ term represents the ground motion incoherence effect. The coherence function used in the Veletsos formulations is,

$$\Gamma\left(|\mathbf{r}_1 - \mathbf{r}_2|, \omega\right) = e^{-\left(\frac{\kappa\omega}{V_S}|\mathbf{r}_1 - \mathbf{r}_2|\right)^2} \tag{2.15}$$

where κ is a dimensionless incoherence factor which reportedly can be quantified by $\kappa/V_S \sim (2\text{-}3)\times10^{-4}$ sec/m (Luco and Wong, 1986).

Coherence functions have been modeled using exponential functions similar to Eq. 2.15 by a number of researchers (Luco and Wong, 1986; Somerville et al., 1991; Novak,

1987). More refined coherence functions defined using five parameters in the regression have been developed by Abrahamson (1988, 1992), who also performed the regression using $\tanh^{-1}(\Gamma)$ instead of Γ. Abrahamson cautions that functional forms of coherence not using $\tanh^{-1}(\Gamma)$ may not be appropriate because Γ is not normally distributed but $\tanh^{-1}(\Gamma)$ is approximately normally distributed. Nevertheless, the exponential coherence function in Eq. 2.15 was retained for this study due to the relative simplicity of its algebraic form and its ability to capture the decay in coherence with increasing separation and frequency (though not in the mathematically ideal form). The primary errors introduced by the use of Eq. 2.15 are overpredictions of coherence at large distances (i.e. > 100 m) and low frequencies (i.e. < 1 Hz) (Novak, 1987).

Using spatial averaging procedures with the cross spectral density function in Eq. 2.14 and the coherence function in Eq. 2.15, Veletsos and Prasad (1989) and Veletsos et al. (1997) developed expressions for the psds of the horizontal (S_x) and torsional (S_ϕ) motions of the base-slab in terms of $S_g(\omega)$ for circular and rectangular foundation geometries, respectively. In the presentation of results, the torsional motions were represented by circumferential motions of the base-slab in the x-direction (i.e. $S_{cir}=r\cdot S_\phi$ for circular foundations and $b\cdot S_\phi$ for rectangular foundations).

The transfer function amplitudes associated with base slab averaging are presented in Fig. 2.13 for circular and rectangular foundations subject to vertically incident incoherent waves, and Fig. 2.14 for nonvertically incident coherent waves. These transfer functions are plotted against the dimensionless frequency parameter $\tilde{a}_0$, which is defined as follows for circular and rectangular footings, respectively,

$$\tilde{a}_0 = a_0\sqrt{\kappa^2 + \sin^2\alpha_v}$$
$$\tilde{a}_0 = \frac{\omega b}{V_S}\sqrt{\kappa^2 + \sin^2\alpha_v} \qquad (2.16)$$

where $a_0 = \omega r/V_S$. The definition of the $\tilde{a}_0$ factor given in Eq. 2.16 for rectangular foundations applies for identical wave incoherence factors κ in the x and y directions.

Figs. 2.13 and 2.14 indicate that the lateral transfer functions ($\sqrt{S_x/S_g}$) for circular and various rectangular geometries are similar, regardless of the type of wave field. The near equivalence of the results for different aspect ratios (a/b) of rectangular foundations suggests that the lateral transfer function primarily depends on the total area of the foundation. This result is a product of the model formulation in which spatial variations of ground motion only result from random incoherence (which is assumed to be identical in both horizontal directions) or nonvertically incident waves. That is, the effects of "traveling waves," which might result in a temporal incoherence of incident waves across a foundation, has not been considered. Such effects would be sensitive to the plan angle of propagation of the traveling waves relative to the foundation and the aspect ratio of the foundation (but might only be significant for very large foundations).

The torsional transfer function results show a relatively high degree of sensitivity to a/b and the type of wave field. Higher torsional motions occur for lower a/b and nonvertically incident coherent wave fields.

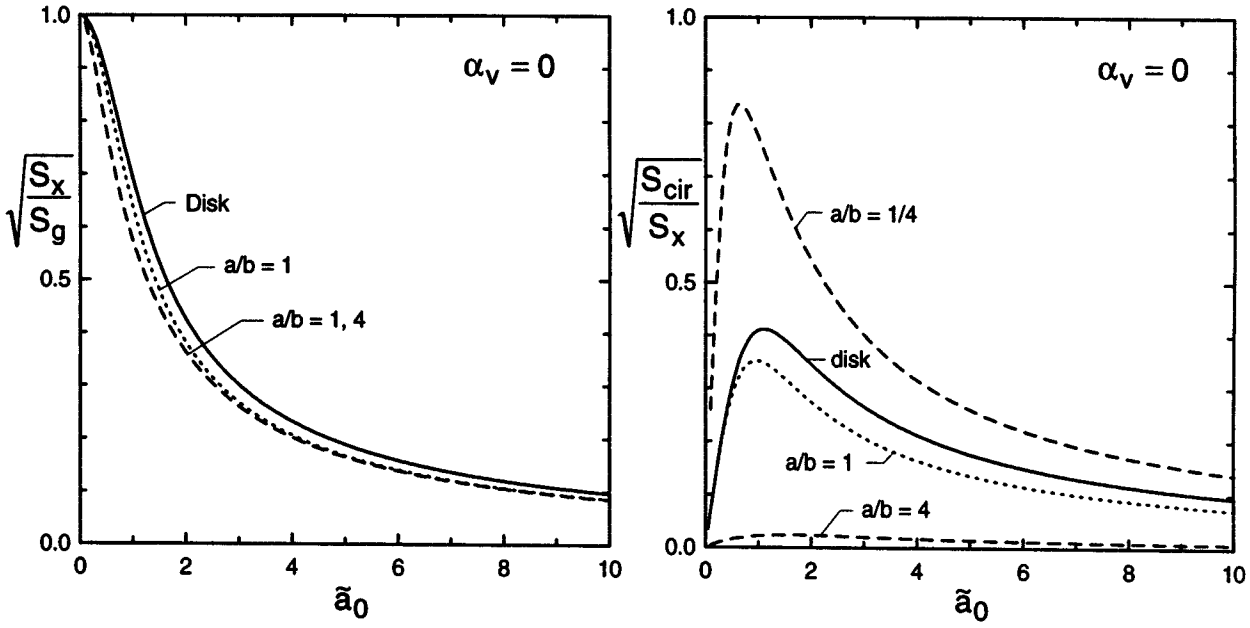

Fig. 2.13: Magnitudes of transfer functions between free-field ground motion and FIM for vertically incident incoherent waves (Veletsos et al., 1997 and Veletsos and Prasad, 1989)

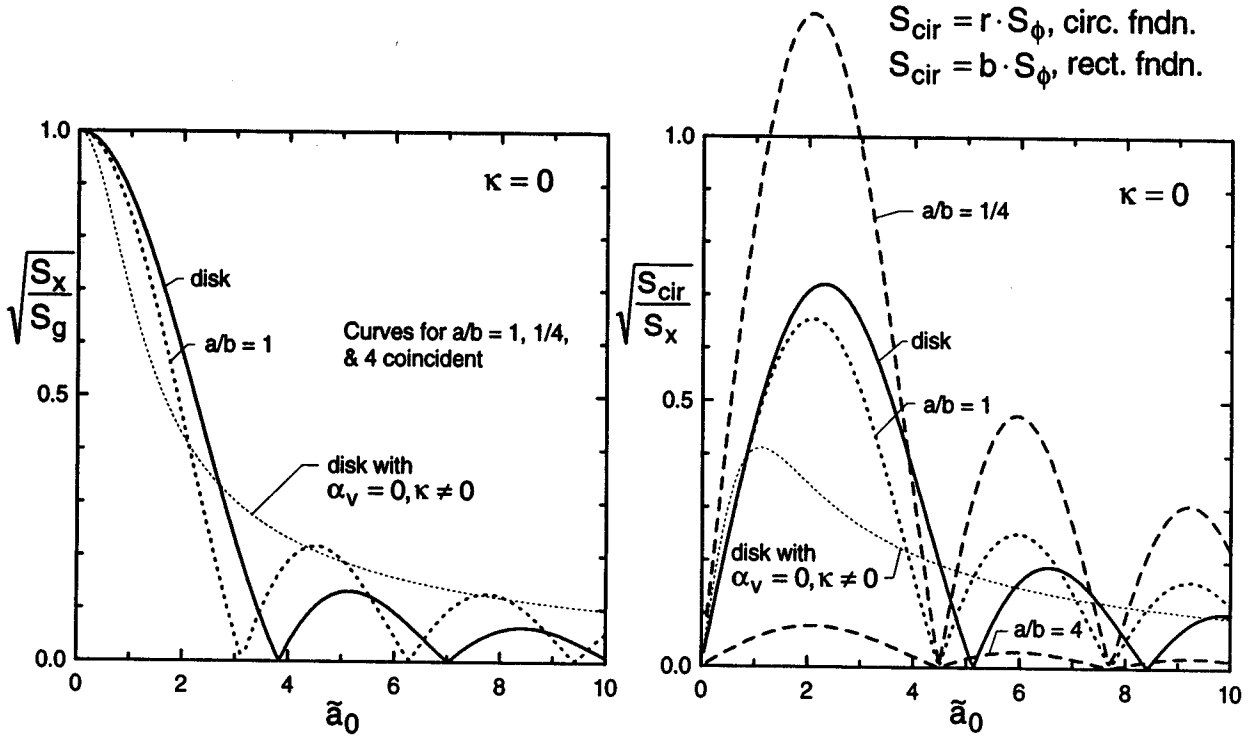

Fig. 2.14: Magnitudes of transfer functions between free-field ground motion and FIM for obliquely incident coherent waves. Curves for disk and vertically incident incoherent waves also shown for comparison (Veletsos et al., 1997 and Veletsos and Prasad, 1989)

2.3.2 Embedment

When subjected to vertically propagating coherent SH waves, embedded foundations experience a reduction in base-slab translational motions relative to the free-field, and rocking motions are introduced. This rocking is not a product of base moment associated with structural inertia, as structure and foundation masses are neglected in the analysis of kinematic interaction. Rather, the rocking is caused by incompatible shear strains along the sides of the excavation and the free-field. Roesset (1980) suggests that these embedment effects are likely to be significant for e/r greater than about 0.15. Analytical and empirical studies have been performed to examine embedment effects on foundation input motions (FIMs), the results of which are presented in the following sections.

(a) *Analytical studies*

Analytical studies of embedment effects have focused on the evaluation of transfer functions expressing the amplitude ratio of base-slab translational and rocking motions to free-field motions (e.g. Elsabee and Morray, 1977 and Day, 1977). These formulations are generally based on assumed vertically propagating coherent waves, so that the base-slab averaging effects discussed in Section 2.3.1 are negligible.

Day (1977) used finite element analyses to evaluate the base motions of a rigid cylindrical foundation embedded in a uniform elastic half space ($\beta = 0$, $\nu = 0.25$) and subjected to vertically incident, coherent SH waves. Elsabee and Morray (1977) performed similar studies but for the case of a visco-elastic soil layer of finite depth over a rigid base ($\beta = 0.05$ and $\nu = 0.33$). The amplitude of the transfer functions for translation and rocking are shown in Fig. 2.15 for the halfspace and Fig. 2.16 for the

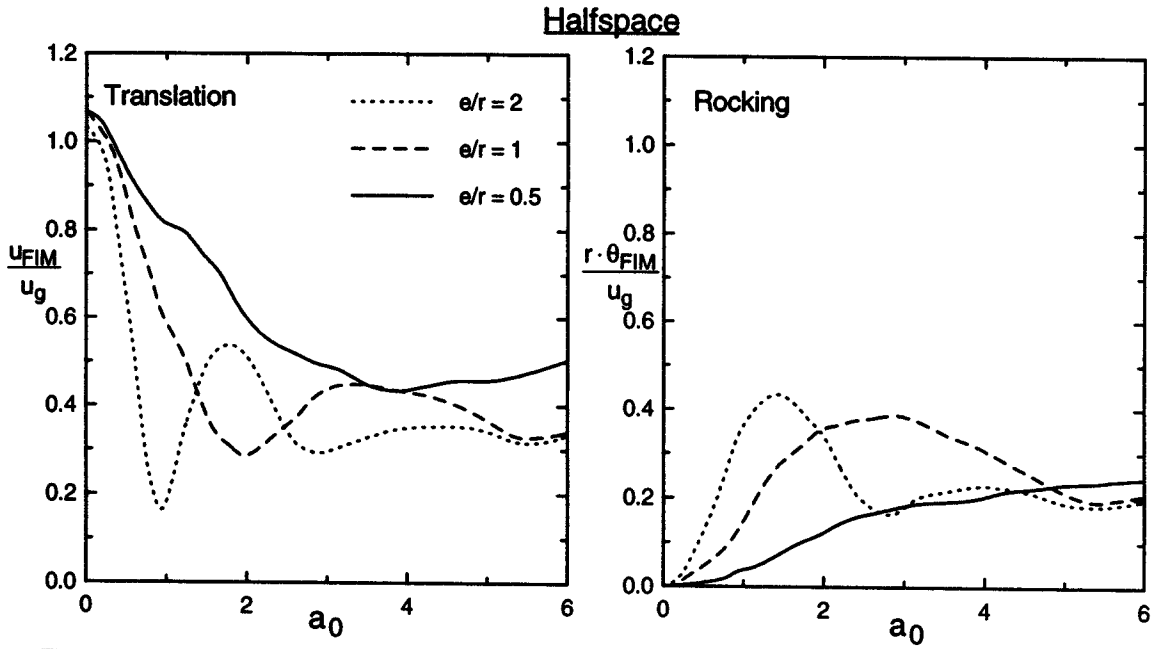

Fig. 2.15: Amplitudes of transfer functions between free-field ground motion and FIM for rigid cylindrical foundation embedded in elastic halfspace and subjected to vertically incident coherent waves (Day, 1977)

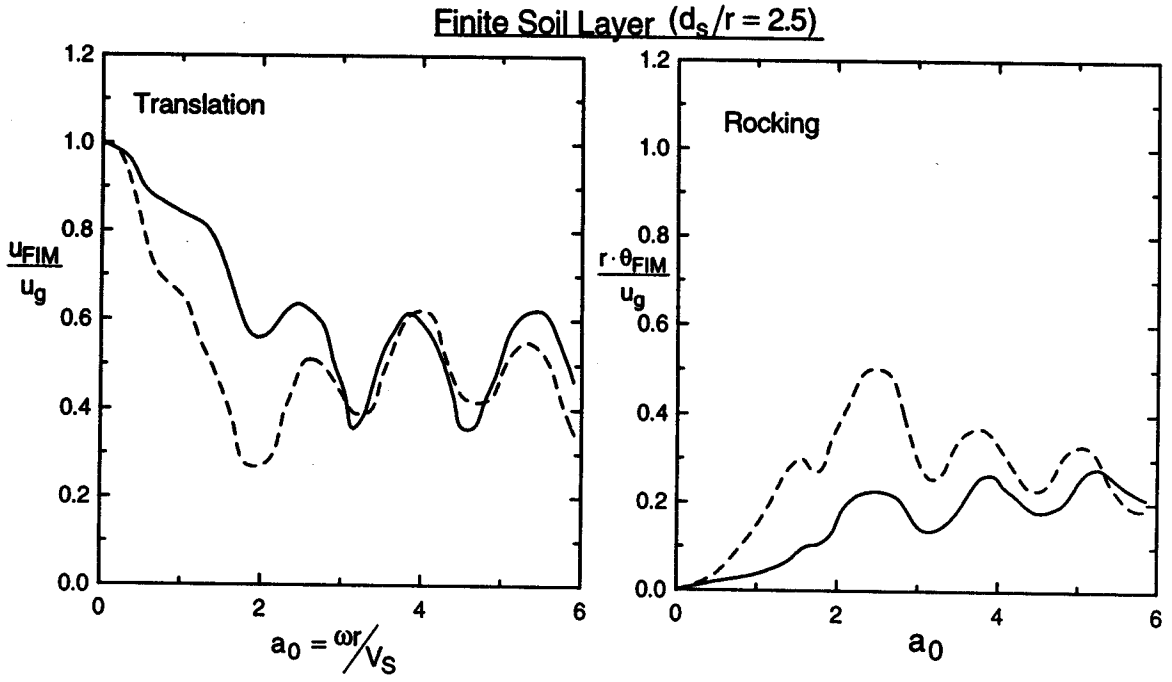

Fig. 2.16: Amplitudes of transfer functions between free-field ground motion and FIM for rigid cylindrical foundation embedded in finite soil layer over rigid base and subjected to vertically incident coherent waves (Elsabee and Morray, 1977)

finite soil layer. The only significant differences between the finite soil layer and halfspace results are high frequency ($a_0 > 1.5$) oscillations in the finite soil layer case. The results for embedment ratios e/r = 0.5, 1.0, and 2.0 (halfspace) and 0.5 and 1.0 (finite soil layer) indicate significant filtering of translational motions for $a_0 > 0.5$ and the development of significant rocking for $a_0 > 1$. At low frequencies ($a_0 < 1.5$), the filtering of foundation motions and the magnitude of rocking motions increases with increasing embedment ratio, while at higher frequencies there is little sensitivity to embedment ratio. These results can be contrasted with the behavior of a surface foundation which would have no reduction of translational motions and no rocking motions when subjected to vertically incident coherent shear waves.

As part of the work by Elsabee and Morray, approximate transfer functions were proposed for the translation and rocking motions of the circular foundation as follows,

translation:
$$|H_u(\omega)| = \begin{cases} \cos\left(\frac{e}{r}a_0\right) & a_0 \le 0.7 \cdot \bar{a}_0 \\ 0.453 & a_0 > 0.7 \cdot \bar{a}_0 \end{cases} \tag{2.17}$$

rocking:
$$|H_\theta(\omega)| = \begin{cases} \frac{0.257}{r}\left(1 - \cos\left(\frac{e}{r}a_0\right)\right) & a_0 \le \bar{a}_0 \\ \frac{0.257}{r} & a_0 > \bar{a}_0 \end{cases} \tag{2.18}$$

where $\bar{a}_0 = \pi/2 \cdot r/e$. Normalized frequency $\bar{a}_0$ corresponds to the fundamental frequency of the soil from the surface to depth e ($\bar{a}_0 = 2\pi f_1 r/V_S$ where $f_1 = V_S/4e$). In Fig. 2.17, these approximate transfer functions are compared to the halfspace (Day, 1977) and finite soil layer (Elsabee and Morray, 1977) solutions for embedment ratios of e/r = 0.5, 1.0, and 2.0. The approximation is reasonable for each embedment ratio and both profiles.

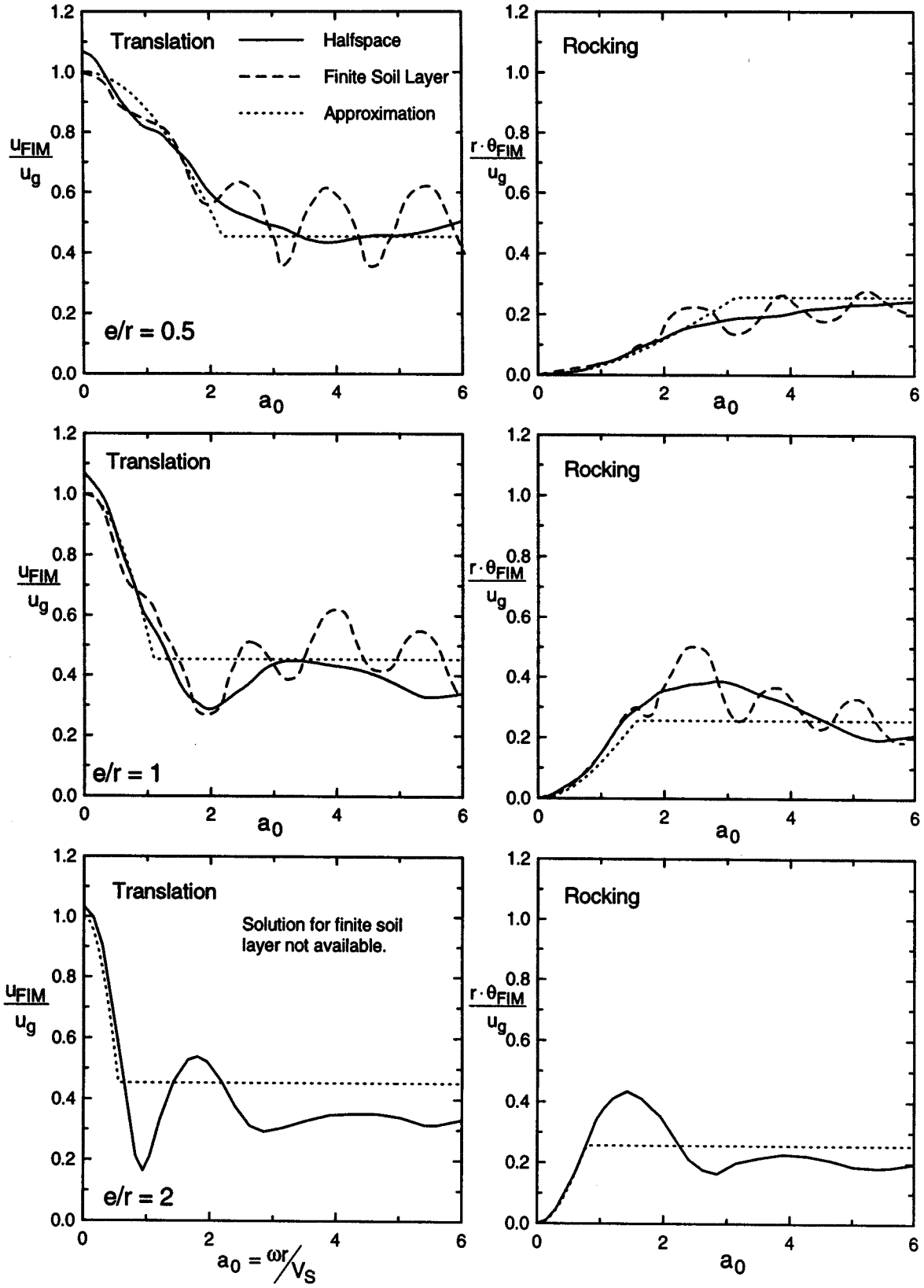

Fig. 2.17: Comparison of transfer function amplitudes for cylinders embedded in a halfspace and finite soil layer and approximation by Elsabee and Morray (Day, 1977 and Elsabee and Morray, 1977)

These results for an embedded rigid cylinder subjected to vertically incident coherent SH waves have been extended for cases of (1) soil properties varying with depth (Elsabee and Morray, 1977), (2) horizontally propagating coherent SH waves (Day, 1977), and (3) non-circular foundations (Mita and Luco, 1989) as follows:

- For soil properties which vary with depth, Elsabee and Morray found that the approximate transfer functions in Eq. 2.17-2.18 remain valid provided an averaged V_S across the embedment depth is used.
- For the case of horizontally propagating coherent SH waves, Day found that the base rocking was practically negligible, the filtering of horizontal motions was significant but was relatively insensitive to e/r, and a significant torsional response was induced at high frequencies ($a_0 > 1.5$). It should be noted, however, that horizontally propagating shear waves are generally of negligible engineering significance in SSI problems because components of ground motion with frequencies above about 1 Hz tend to attenuate rapidly with distance (Chen et al., 1981).
- Mita and Luco found that an embedded square foundation could be replaced by an equivalent cylinder without introducing significant error. The radius of the equivalent cylinder was defined as the average of the radii necessary to match the area and moment of inertia of the square base.

(b) *Empirical studies*

Studies by Seed and Lysmer (1980), Chang et al. (1985), and Johnson and Asfura (1993) have documented reductions in ground motion with depth using both downhole free-field arrays and comparisons of basement and free-field motions. These data are not

repeated here; however, it is noted that both data sets (free-field/downhole and free-field/basement) consistently indicated reductions of peak ground acceleration and high frequency spectral ordinates with depth. It was also concluded by Seed and Lysmer that deconvolution analytical procedures which assume vertically propagating shear waves (e.g. the computer program SHAKE, Schnabel et al., 1972) simulate these effects reasonably well.

Ishii et al. (1984) developed empirical transfer functions for translational motions using earthquake recordings from 18 partially buried tanks in Japan. However, the regression analyses did not include e/r as a variable. Hence the results are likely of limited value as e/r appears to be significant based on the analytical studies discussed in Part (a).

Most structures are not instrumented sufficiently at the foundation-level to measure base rocking, so relatively little data on this effect is available. Even for structures which are instrumented to record base rocking, separation of the kinematic and inertial rocking effects would be impossible without making assumptions about the foundation impedance and wave field, so purely empirical transfer functions for kinematic base rocking are difficult to formulate and have not been developed to date.

2.4 Summary

In this chapter, a number of simplified analytical techniques have been presented for performing both inertial and kinematic SSI analyses. The intent of these analysis procedures is to predict period lengthening ratios and foundation damping factors (inertial

interaction) and foundation/free-field transfer functions (kinematic interaction). Key aspects of these analytical procedures are summarized below.

2.4.1 Inertial Interaction

For analyses of inertial interaction effects, the objectives are predictions of first-mode period lengthening $\tilde{T}/T$ and foundation damping factor $\tilde{\zeta}_0$. The necessary input parameters are:

- Soil conditions: characterization of the site as a halfspace or finite soil layer over rigid base; shear wave velocity V_S and hysteretic damping ratio β which are representative of the site stratigraphy and the level of ground shaking; representative soil Poisson's ratio ν.
- Structure/Foundation Characteristics: effective height of structure above foundation level, h; embedment, e; foundation radii which match the area and moment of inertia of the actual foundation, r_1 and r_2; appropriate corrections to the foundation impedance for embedment, shape, and flexibility effects.
- Fixed Base 1st Mode Parameters: period and damping ratio, T and ζ.

Using these data, the following steps are carried out:

1. Evaluate the foundation impedance function at an assumed period for the flexible-base structure $\tilde{T}$. Static foundation stiffnesses are computed first according to Eq. 2.5 with appropriate modifications for finite soil layer and embedment effects (Eqs. 2.6 and 2.7). Dynamic coefficients α_u, α_θ, β_u, and β_θ are then evaluated for the assumed $\tilde{T}$ using equations in Veletsos and Verbic (1973) with appropriate

modifications to β_θ to account for foundation shape effects, and to α_θ and β_θ to account for flexible foundation effects.

2. Calculate dimensionless parameters σ and γ using Eqs. 2.12 and 2.13. For most structures, it is assumed that $\gamma = 0.15$.
3. Estimate the period lengthening and damping using Eqs. 2.10 and 2.11, calculate a new estimate of $\tilde{T}$.
4. Repeat steps 1 to 3 until the dynamic coefficients α_u, α_θ, β_u, and β_θ are estimated at the actual system period.
5. For embedded foundations, repeat the analyses for $\tilde{T}/T$ and $\tilde{\zeta}_0$ using the formulation by Bielak (1975).

The procedures in steps 1 to 4 are referred to as the "modified Veletsos" formulation. The "modified" term refers to the extension of the basic model considered in Veletsos and Nair (1975) to account for embedded, non-circular, and flexible foundations, and non-uniform soil profiles. Similarly, the Bielak (1975) procedure applied in Step 5 to embedded structures is referred to as the "modified Bielak" formulation.

2.4.2 Kinematic Interaction

For surface foundations, analytical predictions of base-slab averaging effects are made using the transfer functions in Figs. 2.13 and 2.14. A topic of recommended future study is to compare these analytical transfer functions with transfer functions computed from recordings of surface foundation and free-field motion. From such a comparison, the effects of ground motion incoherence and incident wave inclination could be

approximately quantified. Similarly, for embedded structures, the analytical transfer functions in Eqs. 2.17 and 2.18 should be validated against field performance data.